Structure–Composition Relations for the Partly Disordered Hume-Rothery Phase $Ir_{7+7\delta}Zn_{97-11\delta}$ $(0.31 \leq \delta \leq 0.58)$

Wolfgang Hornfeck,[a] Srinivasa Thimmaiah,[a] Stephen Lee,[b] and Bernd Harbrecht*[a]

Abstract: The crystal structure, its variation within the homogeneity range and some physical properties of the new zinc-rich, partly disordered phase $Ir_{7+7\delta}Zn_{97-11\delta}$ $(0.31 \leq \delta \leq 0.58)$ are reported. The structures of three phases with distinct composition were determined by means of single crystal X-ray diffraction. $Ir_{7+7\delta}Zn_{97-11\delta}$ exhibits a significant homogeneity range, adopts a complex γ-brass related cubic structure (*cF*403–406), is stable up to 1201(2) K, and transforms sluggishly below 1048(4) K into a phase with 394 atoms in the monoclinic primitive unit cell. It is a diamagnetic, moderate metallic conductor. Six distinguishable clusters consisting of 22–29 atoms comprise the structure. The clusters are situated about the 16 high symmetry points of the cubic *F* lattice. The structure can be subdivided into two partial structures, one with constant composition $IrZn_5$ and 192 atoms per unit cell and a second being significantly richer in zinc with variable composition and 211–214 atoms per unit cell. The meandering triply periodic minimal surface of two interpenetrating diamond-like nets separates the compositionally variable from its complementary invariant part. The phase width is coupled with substitutional and positional disorder. A comprehensive analysis of composition-dependent site occupancy factors reveals a linear correlation between the various types of disorder which can be conclusively interpreted in terms of an incoherent intergrowth of distinctive partial structures in variable proportions on a length scale comparable to the size of the approximately 2 nm large unit cell. On the basis of the structural findings we derive the structure chemically meaningful formula $Ir_{7+7\delta}Zn_{97-11\delta}$ which quantitatively accounts for the interrelation between substitutional and positional disorder and provides a measure for the homogeneity range in structural terms.

Keywords: Hume-Rothery phases · iridium · structure–composition relations · X-ray diffraction · zinc

Introduction

The average number of valence electrons per atom *e*/*a*, frequently called valence electron concentration *vec*, has been shown by various experimental and theoretical means to be crucial for the sequences of phases and the crystal structures which are preferentially found in noble metal alloy systems comprising a suitable element of Groups 12–15 as a second constituent. Intermetallic phases gaining the decisive part of the stability from this particular electronic factor are usually referred to as Hume-Rothery alloys or electron phases.[1,2]

The mechanism underlying the *e*/*a*-scaled stabilization of crystal structures has been explained in terms of a lowering of the kinetic energy of the valence electrons associated with a reduction of the density of states at the Fermi level. Following Jones' analysis,[3] such a reduction is expected at a given *vec* value for that type of structure which affords energetically favorable flat portions at the Fermi surface, due to contacts between the free electron Fermi sphere of diameter $2k_F$ with a suitable set of Brillouin zones, characterized by the reciprocal lattice vector K_{hkl}.[4,5] As a consequence, the strength of the stabilizing Fermi sphere–Brillouin zone interaction correlates directly with the valence electron concentration. Moreover, the proposed mechanism implies that the energetically favorable structure does not depend on any other element-specific property of the chemical constituents but the number of chemically active valence electrons. The sequence of the elemental structure types like face-centered cubic, body centered cubic and hexagonal close packed being frequently found in Hume-Rothery systems has been rationalized this way.[2,6] An often cited text book example reflecting the *e*/*a*-scaled stabilization is the series of β-brass-type structures CuZn, $AlCu_3$, and Cu_5Sn: All three phases

[a] Dipl.-Chem. W. Hornfeck, M. Sc. S. Thimmaiah, Prof. Dr. B. Harbrecht
Department of Chemistry and Center of Material Sciences
Philipps University Marburg, 35032 Marburg (Germany)
Fax: (+49) 6421 28 28 917
E-mail: harbrecht@chemie.uni-marburg.de

[b] Prof. S. Lee
Department of Chemistry, Baker Laboratory
Cornell University, Ithaca NY 14852-1301 (USA)

Supporting information for this article is available on the WWW under http://www.chemeurj.org/ or from the author.

DOI: 10.1002/chem.200400059

have $^3/_2$ chemically active electrons per atom available for bonding. All three phases adopt the *bcc* W-type structure irrespective of the structural distinctions of the constituents.

Structurally more complex phases occur in many brass-like systems in phase fields at *vec* values of about $\frac{21}{13}$ *e*/*a*. The atomic arrangements of these so-called γ-phases are frequently discussed in terms of cooperatively distorted, ordered defect variants of W-type β-brass-like structures.[7] Although the prototypic structure of γ-Cu_5Zn_8 is known since the early days of X-ray crystallography,[8] structurally related phases have attracted the interest of scientists over decades due to their intricate structural and physical properties. Among these are a substantial number of Al-, Mg-, and Zn-rich phases exhibiting γ-brass related, complex structures with 396 to 448 atoms in a face-centered cubic unit cell of about 2 nm edge length. For a structural chemist, atomic architectures of such a degree of complexity pose the question to which extent and how element-specific properties bias the structural outcome in these systems beyond Hume-Rothery's *vec* correlation. Recently discovered and/or characterized phases are $Al_{69}Ta_{39}$,[9] $(Fe,Zn)Zn_{6.5}$,[10] Ir_4Mg_{29},[11] $MoZn_{20.44}$,[12] and Pt_5Zn_{21}.[13] In spite of compositional and structural dissimilarities the structures can uniformly and favorably be visualized by decomposing them into four symmetrically independent structural units each comprising 22–29 atoms and being grouped about one of the high symmetry points at 000, $\frac{1}{4}\frac{1}{4}\frac{1}{4}$, $\frac{1}{2}\frac{1}{2}\frac{1}{2}$, $\frac{3}{4}\frac{3}{4}\frac{3}{4}$ or equivalent positions.

Subject of this account is a novel γ-brass related phase of composition $Ir_{7+7\delta}Zn_{97-11\delta}$ ($0.31 \le \delta \le 0.58$) which we uncovered in the Zn-rich domain of the Ir–Zn system as a result of our ongoing investigations on expressions of structural complexity in intermetallic systems.[13–16] Comprehensive single crystal X-ray diffraction studies of various specimens covering the whole homogeneity range of the phase revealed a before unseen structure–composition relation for a structurally highly differentiated alloy. We shall show that the formula $Ir_{7+7\delta}Zn_{97-11\delta}$ ($0.31 \le \delta \le 0.58$) adequately reproduces the homogeneity range as well as essential structural characteristics. Moreover, it reflects the ostensible coherency between substitutional and positional disorder which severely affects the structure of this partly disordered high temperature phase.

Results and Discussion

Homogeneity range, thermal stability, magnetic and electrical properties: $Ir_{7+7\delta}Zn_{97-11\delta}$ is a new Zn-rich phase with an extended phase width ranging from about $Ir_{9.2}Zn_{93.6}$ to $Ir_{11.1}Zn_{90.6}$. It represents a structurally distinctive member of a class of γ-brass related intermetallic phases; the structures are composed of 396 to 448 atoms contained in a nearly 2 nm large cubic face-centered unit cell.[17] $Ir_{7+7\delta}Zn_{97-11\delta}$ forms readily upon melting appropriate mixtures of the elements ($0.080 \le x_{Ir} \le 0.120$, x_{Ir}: molar fraction of Ir) at 1373 K, followed by quenching the sample in cold water after annealing the solidified product at 1073 K for several hours.

$Ir_{7+7\delta}Zn_{97-11\delta}$ is metastable at ambient temperature. Thermal analyses combined with X-ray diffraction proved for two single phase samples ($x_{Ir} = 0.085$, $x_{Ir} = 0.110$) that the thermally quenched cubic phase reversibly transforms during a thermal treatment for two hours at 873 K into a monoclinic phase (*P*2/*n*, Pearson symbol: *mP*394, *a*: 1978.3(2), *b*: 911.7(1), *c*: 3223.4(2) pm, β: 96.33(1)°, IPDS data).[18] As seen from Figure 1, the monoclinic-cubic phase

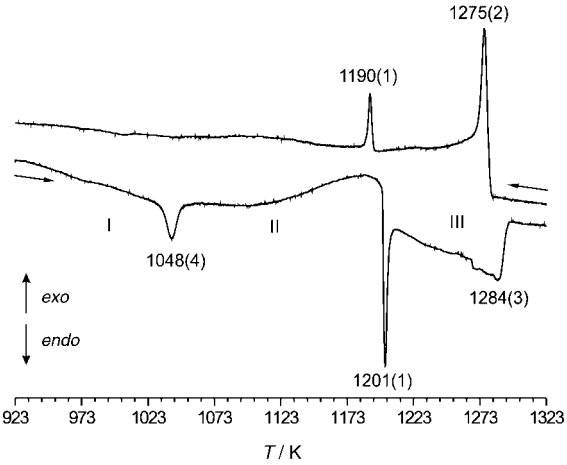

Figure 1. Thermochemical analysis of $Ir_{7+7\delta}Zn_{97-11\delta}$ ($x_{Ir} = 0.085$). Shown are the thermal stability ranges of cubic $Ir_{7+7\delta}Zn_{97-11\delta}$ (II), the monoclinic phase (I), and the γ-type phase (III) together with the respective phase transition temperatures.

transition I→II is accompanied by an endothermic event occurring at 1048(4) K. A second peak at 1201(1) K indicates the upper thermal stability limit of the phase. At this temperature $Ir_{7+7\delta}Zn_{97-11\delta}$ seems to transform into a structurally less differentiated, ordinary γ-brass-type phase (III). This is concluded from X-ray diffraction experiments performed at ambient temperature on samples rapidly quenched from 1223 K. Moreover, the transition triggers the onset of incongruent melting which is completed at 1284(3) K. Upon cooling, the sample re-crystallizes at 1275(2) K. $Ir_{7+7\delta}Zn_{97-11\delta}$ forms back at 1190(1) K. It resists conversion into the monoclinic phase at a cooling rate of 10 K min^{-1}. We annotate that technical problems due to the volatility of zinc hamper an unambiguous clarification of the phase relations above 1200 K. Further details are given in the Experimental Section.

The magnetic properties of the γ-brass related Zn-rich phases are apparently dominated by the core diamagnetism of its constituents. Samples of nominal composition $x_{Ir} =$ 0.080, 0.100, 0.110 have molar susceptibilities χ_{mol} per atom which drop steadily with increasing iridium content from −3.41(1), over −3.18(1) to $-2.98(3) \times 10^{-10}$ m^3 mol^{-1}. This trend continues for the adjacent γ-phase Ir_2Zn_{11} ($-0.55(1) \times 10^{-10}$ m^3 mol^{-1}) for which the Pauli paramagnetism of the conduction electrons almost compensates all diamagnetic contributions.

$Ir_{7+7\delta}Zn_{97-11\delta}$ shows resistivities ρ steadily growing from 1.25 mΩ cm (12 K) to 1.85 mΩ cm (293 K). These values are nearly three orders of magnitude higher than that of zinc metal ($\rho(293\text{ K}) = 5.8$ μΩ cm). An anomalous conductivity spike occurs reproducibly at about 35 K upon heating (cf. Figure 2). Up to now the origin of the spike cannot be explained on the basis of available data.

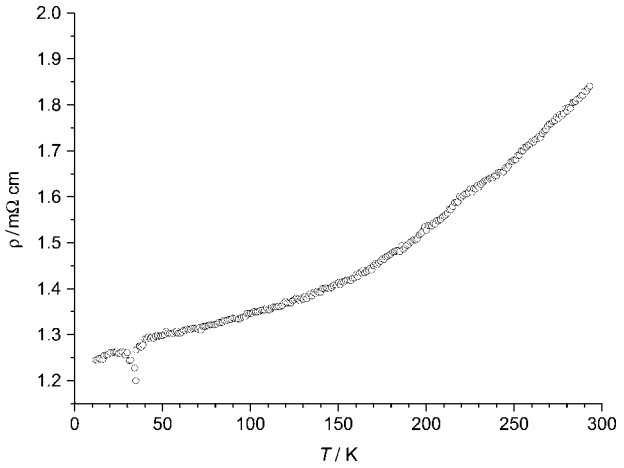

Figure 2. Resistivity ρ of single phase $Ir_{7+7\delta}Zn_{97-11\delta}$ ($x_{Ir}=0.100$) between 12 and 293 K.

Structural characteristics: $Ir_{7+7\delta}Zn_{97-11\delta}$ $(0.31 \leq \delta \leq 0.58)$ forms a complex, partly disordered structure which can be seen as consisting of structural units as present in tungsten (β-brass, respectively), α-manganese,[19–21] γ-brass,[8] and Ti_2Ni.[22] The phase crystallizes in the acentric space group $F\bar{4}3m$ with approximately 403 to 406 atoms in the cubic unit cell. The mean number of atoms in the unit cell increases parallel to the zinc content, whereas the unit cell volume barely changes with composition. Obviously, the shrinkage of the volume coming along with the increasing number of vacancies with increasing iridium content of the phase is balanced by the larger atomic volume of iridium (10.47×10^6 pm^3) compared with that of zinc (9.97×10^6 pm^3). $Ir_{7+7\delta}Zn_{97-11\delta}$ (*cF*406–403) forms a $(2a_\gamma)^3$ derivative structure to the ordinary γ-type phase Ir_2Zn_{11}[23] (*cI*52) which in turn represents a $(3a_{bcc})^3$ superstructure of the elemental *bcc*-type structure (*cI*2). Hence, $Ir_{7+7\delta}Zn_{97-11\delta}$ can be conceived as a *bcc* variant of order 216 ($\hat{=}(6a_{bcc})^3$).

One method of description having been applied to related structures effectively analyzes the structures in terms of the underlying three-dimensional connected frameworks by means of invariant lattice complexes.[24,25] A second, more commonly used description focuses on the local arrangements of sets of symmetrically independent atoms grouped around sites of maximal point symmetry. Such atomic sets have been termed clusters,[7] sets of nested polyhedra,[25] or nested polyhedra units.[26] We choose the second method for extracting structural characteristics of this new binary Zn-rich phase from the positional parameters determined by single crystal X-ray diffraction means for three distinctly composed crystals. Subsequently we shall use the term cluster well knowing that we do not address the question of chemical bonding in the selected atomic sets. Nevertheless, the purely geometric description of the structure in terms of specific atomic aggregates receives its justification from the fact that it concisely visualizes constitutive structural features and uncovers distinctive structural properties in an easy recognizable way.[26] According to this concept each cluster is defined by a sequence of three or four symmetrically independent atomic sites arranged in polyhedral shells around an occupied or empty center of high symmetry. The shells are congruent to one of the Platonic or Archimedean solids. They are distinguished by two capital letters: IT stands for inner tetrahedron, OT for outer tetrahedron, OH for octahedron, CO for cuboctahedron, and TT for truncated tetrahedron. Considering relative orientations, the IT and OT sites together constitute a more or less distorted cube, while the OT and TT sites build up a 16 atoms cluster which is known as Friauf polyhedron. CC denotes the center of a cluster. Such centers are located at 000, $\frac{1}{4}\frac{1}{4}\frac{1}{4}$, $\frac{1}{2}\frac{1}{2}\frac{1}{2}$, $\frac{3}{4}\frac{3}{4}\frac{3}{4}$ and equivalent translational invariant points. Hence, the structures are built up by 4×4 clusters. Table 1 lists some typical representatives of γ-brass related superstructures and their decomposition into the characteristic clusters. Most of the

Table 1. Selected $(2a_\gamma)^3$ derivative structures with isolated cluster units (space group: $F\bar{4}3m$).

Compound	*cF*…	*a*/pm	Cluster types[a]				Ref.
			γ	Ti_2Ni	α-Mn	Ti_2Ni	
Mg_6Pd	396	2010.8(2)	$Pd_4^{OT}Mg_{22}$	$Pd_4^{OT}Mg_{18}$	Mg_{29}	$Pd_4^{OT}Mg_{18}$	[39]
Ir_4Mg_{29}	396	2011.48(3)	$Ir_4^{OT}Mg_{22}$	$Ir_4^{OT}Mg_{18}$	Mg_{29}	$Ir_4^{OT}Mg_{18}$	[11]
			γ	γ	α-Mn(−CC)	Ti_2Ni	
Ir_7Mg_{44}	408	1871.0(2)	$Ir_4^{OT}Mg_{22}$	$Ir_6^{OH}Mg_{20}$	Mg_{28}	$Ir_4^{OT}Mg_{18}$	[40]
$Fe_{22}Zn_{78}$	408	1796.3(10)	$Fe_8^{IT,OT}Zn_{18}$	$Fe_{14}Zn_{12}^{CO}$	Zn_{28}	$Fe_4^{OT}Zn_{18}$	[41]
			γ	*bcc*/γ	α-Mnγ(−CC)	Ti_2Ni	
$(Fe,Ni)Zn_{6.5}$	408	1808.38(53)	Zn_{26}	$(Fe,Ni)_{10.68}^{CC,OT,OH}Zn_{16}$	Zn_{29}	$(Fe,Ni)_4^{OT}Zn_{18}$	[10]
			γ	*bcc*/γ	α-Mn/γ	Ti_2Ni	
$Ir_{7+7\delta}Zn_{97-11\delta}$	406–403	1822.1(4)	$Ir_4^{OT}Zn_{22}$	$Ir_{1-\delta+m}^{CC,OT,OH}Zn_{26-m}$	$Zn_{29-3\delta}$	$Ir_4^{OT}Zn_{18}$	
			γ	γ	α-Mn(−CC)	Ti_2Ni	
Na_6Tl	412	2415.4(1)	$Tl_4^{OT}Na_{22}$	$Tl_8^{IT,OT}Na_{18}$	Na_{28}	$Tl_4^{OT}Na_{18}$	[42]
			bcc′ [b]	*bcc*′	α-Mn(−CC)	Ti_2Ni	
$MoZn_{20.44}$	420	1846.4(1)	$Zn_{24.05}$	$Mo^{CC}Zn_{21.96}$	Zn_{29}	$Mo_4^{OT}Zn_{18}$	[12]
			bcc′	α-Mn	α-Mn	γ	
$Al_{69}Ta_{39}$	432	1915.3(10)	$Ta^{CC}Al_{23}$	$Ta_{12}^{TT}Al_{17}$	$Ta_5^{CC,OT}Al_{24}$	$Ta_{16}^{OT,CO}Al_{10}$	[9]
			bcc	α-Mn	α-Mn	*bcc*	
$Cd_{45}Sm_{11}$	448	2169.9(3)	$Sm_4^{OT}Cd_{23}$	$Sm_{13}^{CC,CO}Cd_{14}$	$Sm^{CC}Cd_{28}$	$Sm_4^{OT}Cd_{25}$	[43]
$Cu_{41}Sn_{11}$	416	1798.0(7)	$Sn_4^{OT}Cu_{22}$	$Sn_{12}^{CO}Cu_{14}$	Cu_{26}	$Sn_6^{OH}Cu_{20}$	[44]
$Li_{21}Si_5$	416	1871.0(2)	$Si_4^{OT}Li_{22}$	$Si_6^{OH}Li_{20}$	$Si_6^{OH}Li_{20}$	$Si_4^{OT}Li_{22}$	[45]
Pt_5Zn_{21}	416	1809.1(1)	$Pt_4^{OT}Zn_{22}$	$Pt_{6-\delta}^{OH}Zn_{20+\delta}$	$Pt_{6-\delta}^{OH}Zn_{20+\delta}$	$Pt_4^{OT}Zn_{22}$	[13]

[a] Cluster types presented as sequence along a selected body diagonal with the choice of origin and cluster orientation corresponding to that of $Ir_{7+7\delta}Zn_{97-11\delta}$. [b] *bcc*′ denotes *bcc*-type clusters with partly occupied sites.

entries were taken from a collection of phases previously assorted by Hellner.[25]

The single crystal structure refinements display that the atomic arrangement can be subdivided into two partial structures of similar size but substantially different composition. One partial structure is completely ordered and compositionally invariant throughout the whole homogeneity range of the phase (Table 2). It comprises 192 atoms and two different cluster types. The composition of the clusters situated at the chosen origin (000, position 1)—and sym-

Table 2. Structural data for $Ir_{7+7\delta}Zn_{97-11\delta}$ ($\delta = 0.31, 0.38, 0.58$).

Cluster	Atom	Site		x	y	z	SOF	U_{eq}[a]/pm^2
1	Zn11	16e	IT	0.05309(14)[b]	x	x	1	95(9)
				0.05294(15)				133(8)
				0.05297(10)				126(5)
	Ir12	16e	OT	0.91350(4)	x	x	1	36(3)
				0.91334(4)				57(3)
				0.91316(3)				43(2)
	Zn13	24f	OH	0.17672(24)	0	0	1	110(8)
				0.17628(23)				139(7)
				0.17743(14)				122(5)
	Zn15	48h	CO	0.15662(11)	x	0.01988(15)	1	125(6)
				0.15597(12)		0.01971(15)		188(6)
				0.15574(8)		0.01904(9)		162(4)
2a/**2b**	Ir20	4c	CC	1/4	1/4	1/4	0.41(2)	126(23)
							0.25(2)	161(39)
				–	–	–	0	–
	Zn21	16e	IT	0.30452(32)	x	x	0.60(3)	86(32)
				0.30387(36)			0.62(5)	64(29)
				0.30423(10)			1	124(5)
	Zn21′	16e	IT′	0.32859(105)	x	x	0.30(4)	551(113)
				0.32533(227)			0.25(6)	565(152)
				–	–	–	0	–
	M22	16e	OT	0.16452(12)	x	x	0.02(2)[c]	69(16)
				0.16454(11)			0.09(2)	107(13)
				0.16438(6)			0.182(10)	57(6)
	M23	24g	OH	0.07969(21)	1/4	1/4	0.10(1)[c]	143(13)
				0.07878(16)			0.16(1)	126(10)
				0.07782(8)			0.377(8)	101(4)
	Zn25	48h	CO	0.08768(19)	x	0.27016(19)	1	290(9)
				0.09021(18)		0.27052(19)		287(8)
				0.09400(8)		0.27173(11)		178(4)
3a/**3b**	Zn30	4b	CC	1/2	1/2	1/2	0.70(5)	177(44)
							0.63(7)	267(61)
							0.51(4)	227(46)
	Zn31	16e	IT	0.57090(52)	x	x	0.42(3)	365(55)
				0.57061(36)			0.45(3)	314(46)
				0.57076(20)			0.64(2)	299(20)
	Zn32	16e	OT	0.41500(15)	x	x	1	88(9)
				0.41590(17)				141(9)
				0.41840(11)				118(5)
	Zn33	24f	OH	0.32345(77)	0	0	0.29(3)	278(63)
				0.32087(57)			0.36(3)	225(42)
				0.32062(24)			0.62(2)	281(19)
	Zn34	48h	TT	0.04735(15)	x	0.65382(26)	0.62(1)	130(13)
				0.04700(18)		0.65423(34)	0.57(2)	215(17)
				0.04687(24)		0.65546(43)	0.33(1)	287(22)
	Zn35	48h	CO	0.18505(22)	x	0.51485(20)	1	343(10)
				0.17617(183)		0.51639(79)	0.40(11)	301(55)
				0.17785(14)		0.51750(11)	1	379(7)
	Zn35′	48h	CO′	–	–	–	0	–
				0.19212(126)	x	0.51272(238)	0.62(11)	256(45)
				–	–	–	0	–
4	Ir42	16e	OT	0.65098(4)	x	x	1	29(3)
				0.65128(4)				57(3)
				0.65199(3)				39(2)
	Zn43	24g	OH	0.63776(25)	1/4	1/4	1	170(8)
				0.63709(26)				216(8)
				0.63667(19)				251(6)
	Zn45	48h	CO	0.10398(11)	x	0.77717(16)	1	130(6)
				0.10404(11)		0.77713(16)		169(5)
				0.10385(7)		0.77673(10)		155(4)

[a] U_{eq} is defined as one third of the trace of the orthogonalized U_{ij} tensor. [b] Structural data given in the top, middle and bottom lines refer to crystal **1**, **2** and **3**, respectively. [c] SOF(Ir), SOF(Zn) = 1−SOF(Ir).

metrically equivalent positions as the centers of the faces—coincides with that of the ordinary γ-phase, Ir_4Zn_{22}.[23] This so-called γ-type cluster **1** is built up by four shells. Next to an unoccupied center we find four zinc atoms (IT), followed by four iridium atoms at OT positions. Six zinc atoms forming an octahedron (OH) are somewhat more distant from the center than the iridium atoms. 12 zinc atoms positioned at the vertices of an distorted cuboctahedron (CO) complete the Ir_4Zn_{22} cluster shown in Figure 3. The second well-ordered cluster consists of three shells: OT, OH, CO. It is grouped about the high symmetry points at, for example, $\frac{3}{4}\frac{3}{4}\frac{3}{4}$ (position 4). Again, the minority component segregates on the OT site slightly above the middle of the edges of an octahedron formed by six zinc atoms. The two shells are sheathed by 12 additional zinc atoms completing a Ti_2Ni-type Ir_4Zn_{18} cluster **4**, see Figure 3. The two cluster types **1** and **4** are arranged like zinc and sulfur atoms in zinc blende. Thus, the partial structure (**1**+**4**) represents a hierarchical, colored version of a diamond-type framework which is shown in blue in Figure 4. This compositionally invariant part of the structure accumulates the largest portion of the minor constituent iridium. Its composition corresponds to $IrZn_5$.

The second partial structure exhibits a noticeable compositional variability ranging from $IrZn_{45.8}$ ($\delta = 0.31$) to $IrZn_{16.5}$ ($\delta = 0.58$). The compositional flexibility of the complementary structural subunits is expressed by three discernible kinds of disorder (cf. Table 2):

i) partial occupation of otherwise empty central cluster positions (e.g. Ir20),
ii) mutual statistical substitution of the two constituents on specific OT and OH sites (e.g. M22),

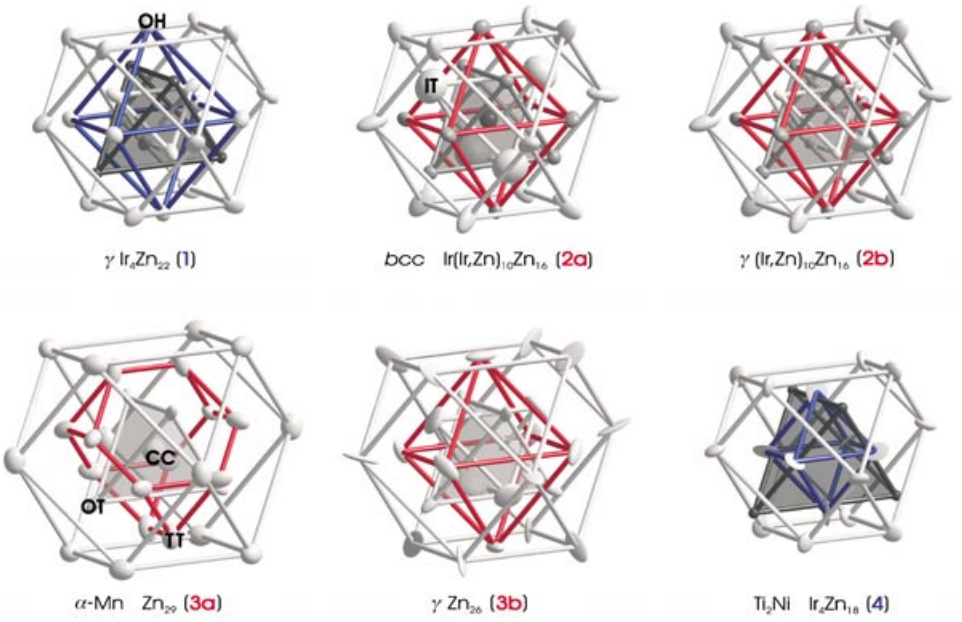

Figure 3. Representation of the six symmetrically and topologically distinct clusters appearing in the crystal structure of $Ir_{7+7\delta}Zn_{97-11\delta}$ ($\delta = 0.38$) along [3$\bar{6}$1]. All atoms are displayed via their anisotropic thermal displacement ellipsoids (90% probability, crystal 2). Ellipsoids representing sites with mixed Ir/Zn occupation are shown in medium grey, those of iridium and zinc in dark and light grey, respectively. Selected shells are labelled with their abbreviations as used throughout the text. The clusters are consecutively numbered according to their occurrence along [111], starting with the ordered γ-type cluster **1** situated about the origin. Each cluster is marked by its symbol and composition. The chosen color-code allows the distinction of clusters constituting a substructure of constant (blue) and variable (red) composition.

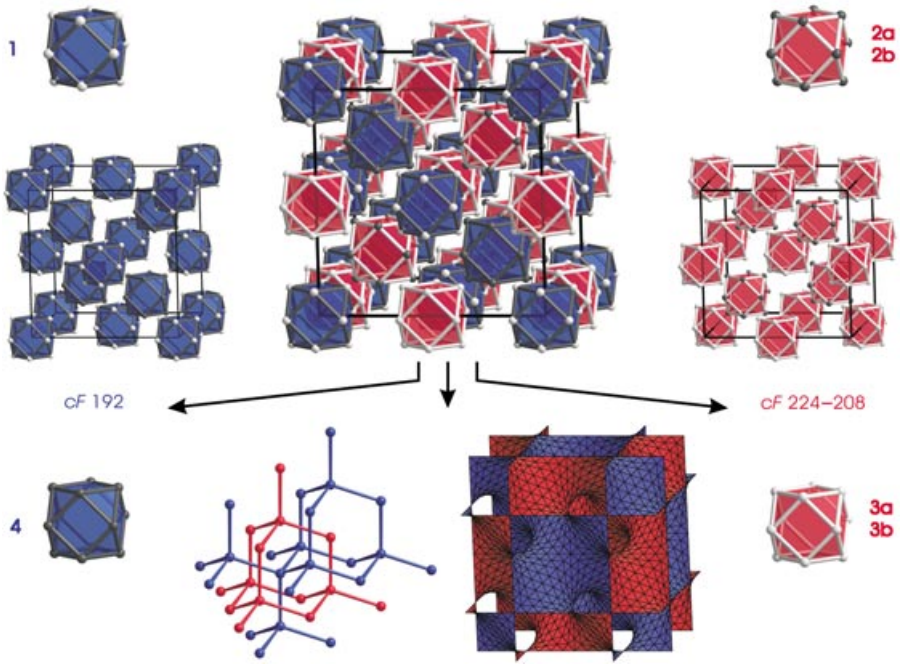

Figure 4. Relative arrangement of clusters at the high symmetric points of the *F*-centered cubic unit cell of $Ir_{7+7\delta}Zn_{97-11\delta}$. The clusters are represented by idealized cuboctahedral shells, which are color-coded regarding their affiliation with either the compositionally invariant (blue, *cF*192-substructure) or variable (red, *cF*224–208) substructure. This dissection of the structure emphasizes the two subsets of clusters forming two interpenetrating diamond-type frameworks embedded in the interwoven labyrinths of the triply periodic *D*-surface (see ref. [28]–[31] and references therein for further information on the *D* surface, and[38] for details concerning the calculation used for this work).

iii) positional disorder in form of split positions (e.g. Zn21/Zn21′, Zn33/Zn34).

The clusters are grouped around $\frac{1}{4}\frac{1}{4}\frac{1}{4}$ (position 2), $\frac{1}{2}\frac{1}{2}\frac{1}{2}$ (position 3), and symmetrically equivalent points. The disorder of type (i) and (iii) gives rise to some physically meaningless short distances. Such problems unravel completely if we assume that two different cluster types alternatively are situated about these high symmetry points. This assumption is corroborated by the pair-wise linear dependence of related site occupancy factors (SOF) of those adjacent atomic sites which produce too short interatomic distances, compare, for example, CC: SOF(Ir20) = 0.41(2) and IT: SOF(Zn21) = 0.60(3) (Table 2). Actually, in no case the sum of SOF of two very close sites exceeds unity. Hence, we may conclude that either β-brass-type $Ir(Ir,Zn)_{10}Zn_{16}$ fragments **2a** composed by CC, IT′, OT, OH and CO sites or γ-type $(Ir,Zn)_{10}Zn_{16}$ clusters **2b** (IT, OT, OH, CO) reside at positions 2. The presence of iridium at the center of cluster **2a** is indicated by the height of the electron density which, for the Ir-rich phase, surmounts the value for a fully occupied zinc site. The proposed distinct partitioning of zinc in clusters **2a**/**2b** is obvious since the OT and OH sites of these two clusters coincide within the accuracy of our calculations. Correspondingly, we find either an α-Mn-type Zn_{29} cluster **3a** or a γ-type Zn_{26} cluster **3b** on positions 3. The α-Mn-type cluster comprises the sites CC, OT, TT and CO, see Figure 3. Correlations between the SOF of positionally disordered, statistically and partly occupied sites indicate that the **2a**/**3a** clusters prevail at the Zn-rich phase boundary whereas the **2b**/**3b** clusters predominate at the Ir-rich phase boundary of $Ir_{7+7\delta}Zn_{97-11\delta}$. Although differing in number of atoms (29 and 26, respectively), the clusters **3a**/**3b** about $\frac{1}{2}\frac{1}{2}\frac{1}{2}$ and equivalent positions consist exclusively of zinc. Therefore, the variation of the iridium content in the whole phase is essentially connected to an exceedingly large compositional flexibility of a rather small structural region inside the cuboctahedral shell of the clusters situated on position 2. In this region the composition varies between $IrZn_{21.8}$ and $IrZn_{7.6}$. Another point noteworthy to mention is the stabilization of an unique α-Mn-type Zn_{29} cluster in a chemically beneficial environment. As in the case of clusters **1** and **4**, the substructure (**2a**/**2b**+**3a**/**3b**) constitutes a second diamond-like framework, shown in red in Figure 4. The two diamond-like nets are shifted by one half of a lattice vector and interpenetrate. Accordingly, the structure topologically represents a hierarchical variant of the cuprite structure (Cu_2O).[27] The two diamond-like skeletal partial structures are spatially separated by a meandering triply periodic minimal surface, known as Schwarz' diamond or *D* surface.[28–31] This intersection-free internal surface separates the compositionally variable partial structure from its invariant counterpart, see Figure 4. Our interpretation of the structural findings implies furthermore, that the flexible part of the structure actually consists of two compositionally distinguishable parts; one being less Zn-rich with 211 and a second being particular rich in zinc with 214 atoms per unit cell. Thus, quite untypical for alloys, the phase width does not primarily arise from a variable mutual replacement of the two distinct chemical constituents on specific atomic sites. Instead, the homogeneity range of this structurally highly differentiated phase seems to result from a statistical distribution, that is, an incoherent intergrowth, of two fairly ordered different partial structures in various proportions on length scales corresponding to small integers of the unit cell edge. Further ordering of the compositionally specifiable tiny domains was ruled out by a meticulous but vain search for additional superstructure reflections.

Structure–composition relations: In the following we elucidate the chosen chemical formula. It accounts for the presence of different forms of disorder and reflects the experimentally observed width of the homogeneity range in structural terms. According to the structural findings the mean chemical composition of the phase is given by the weighted sum of the compositions of the six distinctive clusters **1**, **2a**, **2b**, **3a**, **3b** and **4** (cf. Table 2). If we express the degree of substitutional and positional disorder in clusters **2a**/**2b**, **3a**/**3b** by m and δ, respectively, and the fractions of the clusters by δ and $1-\delta$, the overall composition results from the following six addends:

$$\underbrace{Ir_4Zn_{22}}_{\mathbf{1}} + \underbrace{Ir_{1-\delta}(Ir_mZn_{4-m}Zn_{22})_{1-\delta}}_{\mathbf{2a}} + \underbrace{(Ir_mZn_{4-m}Zn_{22})_{\delta}}_{\mathbf{2b}} + \underbrace{(Zn_{29})_{1-\delta}}_{\mathbf{3a}} + \underbrace{(Zn_{26})_{\delta}}_{\mathbf{3b}} + \underbrace{Ir_4Zn_{18}}_{\mathbf{4}} \quad (1)$$

This summation includes i) a linear dependence of the site occupancy of the central site CC (Ir20) with the frequency $1-\delta$ of cluster **2a** and ii) the presence of one of the cluster pairs **2a**/**3a** or **2b**/**3b** per unit cell. Both assumptions are corroborated by the apparent linear dependence of the respective pairs of SOFs in the homogeneity range of the phase (see Table 2 and Figure 5). Combining the two compositionally constant terms and the four variable terms reduces the expression to:

$$Ir_8Zn_{40} + Ir_{1-\delta+m}Zn_{55-3\delta-m} \quad (2)$$

A closer inspection of the variations of the SOFs with the molar fraction of the constituents reveals a further linear interrelation between the substitutional disorder as expressed by the degree of mutual Ir/Zn replacement m and the positional disorder measured by δ.

As seen from the graph m versus x_{Ir} (Figure 5a) the zinc-rich boundary can not fall below $x_{Ir} = 0.084$. At this value the disorder parameter m becomes 0. In a next step we fix the Ir-rich phase boundary with $m = 4$, thereby implying that the composition of cluster **2b** does not exceed the iridium content of an ordered γ-type cluster, that is, Ir_4Zn_{22}. An analysis of the evolution of the substitutional and positional disorder with increasing iridium content (Figure 5) discloses an interrelation between both quantities of disorder according to:

$$m \approx 8\delta - 2 \quad (3)$$

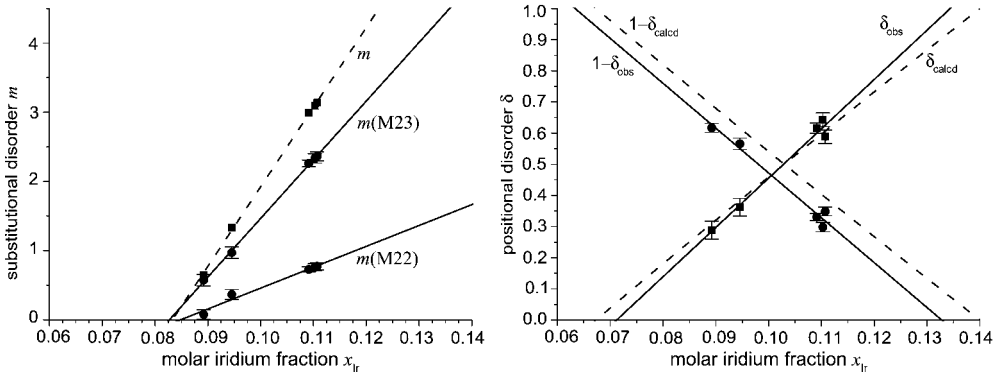

Figure 5. a) Plot of the substitutional disorder parameter m and its components m(M22), m(M23) as a function of the molar iridium fraction x_{Ir}. According to Equation (1) m counts the number of iridium atoms in the γ-type fragment of clusters **2a**/**2b**, thus, m is related to the SOFs of atoms M22 and M23 (cf. Table 2) according to: $m = m(M22) + m(M23) = 4\,SOF(M22) + 6\,SOF(M23)$. A linear regression applied to the data yields $m = 115(2)x_{Ir} - 9.6(2)$. b) Plot of the positional disorder parameter δ and its complementary quantity $1-\delta$ as a function of the molar iridium fraction x_{Ir}. The SOF of Zn33 is chosen to represent δ_{obs}, because Zn33 is uniquely identified with cluster **3b**, where it is situated at the OT site. Correspondingly, Zn34 defining the TT site of the α-Mn-type cluster (cf. Table 2) is characteristic for cluster **3a**. The SOFs of these two atoms are linearly dependent, thereby defining the fractions δ_{obs} and $1-\delta_{obs}$ of the two clusters in the structure at a given molar fraction x_{Ir}. Data evaluation by linear regression gives $\delta_{obs} = 16(1)x_{Ir} - 1.1(1)$ and $1-\delta_{obs} = -14(1)x_{Ir} + 1.9(1)$, respectively. As expected for a complementary relation both curves have similar slopes, differing only in sign. Equations (3) and (4) follow from the $\delta - x_{Ir}$ (b) and the $m - x_{Ir}$ dependences (a). Solving Equation (4) for δ yields the graphs of δ_{calcd} and $1-\delta_{calcd}$.

Combining Equations (2) and (3) yields the formula $Ir_{7+7\delta}Zn_{97-11\delta}$ with $0.25 \le \delta_{calcd} \le 0.75$ corresponding to $0.085 \le x_{Ir,calcd} \le 0.121$. This compares fairly well with the experimentally determined phase width: $0.089(2) \le x_{Ir,obs} \le 0.109(2)$ corresponding to $0.31 \le \delta_{obs} \le 0.58$. Owing to the correlation of the disorder with the homogeneity range of the phase, δ has various meanings:

1) δ and $1-\delta$, respectively, measure the fractions of the cluster pairs **2b**/**3b** and **2a**/**3a**,
2) δ is a quantitative expression of the three types of disorder. For all five crystals we studied, δ reasonably reproduces—irrespective of the type of disorder—the occupational factors of the disordered sites at a given x_{Ir},
3) δ correlates linearly with the molar fraction of the constituents according to:

$$x_{Ir}(\delta) = \frac{n_{Ir}}{n_{Ir}+n_{Zn}} = \frac{7+7\delta}{104-4\delta} \qquad (4)$$

Hence, the range of δ is a measure for the compositional flexibility of the structure.

Although the interrelation between m and δ and its origin are not well understood, the impact of the interdependence of the positional and substitutional disorder on the stability range of the phase is remarkable. As seen from Figure 5a and b, m becomes 0 for $\delta \approx {}^1/_4$. Consequently, there is no suitable matrix adopting exclusively Zn_{26} or Zn_{29} clusters. In accordance with our findings, these two cluster types are only stable if they are chemically intergrown. This feature renders support to the assumption that the m/δ correlation may reflect the structure controlling electronic factor in terms of a Hume-Rothery stabilization. The conventional counting Scheme Ir: −1 electron, Zn: +2 electrons, however, results in *vec* values of 1.73 to 1.67 which are significantly higher than we expect for γ-brass related phases (${}^{21}/_{13} \approx 1.615$). Hence, contrary to the congeneric phase Pt_5Zn_{21},[13] the variation of the composition of $Ir_{7+7\delta}Zn_{97-11\delta}$ does not encompass the typical electron count of a γ-phase, that is, ${}^{21}/_{13}$ electrons/atom.

Our interpretation of the outcome of the structure refinement, namely the postulation of an exceptional mechanism for the evolution of homogeneity ranges in complex intermetallics, is supported by the analysis of effective cluster dimensions throughout the homogeneity range. This is done by a comparison of the circumsphere radii $r_{\mathbf{C}}$ (index **C** representing the cluster number) for respective cuboctahedra, given by the distance between their center (CC site) and their vertices (CO sites). As expected one can see that the dimensions of the compositionally conserved clusters **1** and **4** undergo only slight variations. With increasing iridium content $r_{\mathbf{1}}$ decreases from 405 pm at the Zn-rich side over 404 to 403 pm at the Ir-rich border, while $r_{\mathbf{4}}$ equals 380 pm within the whole range. On the contrary clusters **2a**/**2b** and **3a**/**3b** forming the compositionally variable partial structure, show a greater variation in their effective dimensions. With increasing iridium content a clear decrease of $r_{\mathbf{2a/2b}}$ from 420 pm over 414 to 404 pm (which equals the radius of γ-type cluster **1**) is observable, following the change from the 27 atoms *bcc*-type to the 26 atoms γ-type cluster. Finally $r_{\mathbf{3a/3b}}$ shows the same tendency: starting from 478 pm length (as for both clusters at the Zn-rich side) the radius drops to 460 pm (as for both clusters at the Ir-rich side). In between splitted values were calculated, which allow to estimate the effective dimension for the individual clusters **3a** and **3b** with $r_{\mathbf{3a}}$ of 496 pm for the α-Mn-type and $r_{\mathbf{3b}}$ of 455 pm for the γ-type cluster, respectively. It seems noteworthy to mention that, according to this data, a γ-type cluster constituted solely by zinc includes a 1.4 times larger volume ($r_{\mathbf{3b}} = 455$ pm) than a similar Ir_4Zn_{22} cluster ($r_{\mathbf{1}} = 404$ pm). In view of the similar atomic size, r(Zn) = 133.5 pm and r(Ir) =

135.7 pm with zinc atoms actually being smaller, the huge difference in the cluster sizes can be ascribed to drastically different bonding interaction in the two distinct γ-type fragments.

Conclusions

The Ir–Zn system accommodates in its Zn-rich region a structurally complex, partly disordered phase, Pearson symbol *cF*403–406. The phase transforms below 1048(4) K into a monoclinic phase, *mP*394. The structure of the cubic phase is built up by six distinguishable clusters each comprising 22–29 atoms. The clusters are grouped around the 16 high symmetry points of a cubic *F*-lattice. The structure can be decomposed into two partial structures of comparable size, one being compositionally invariant over the homogeneity range (192 atoms) and a second exhibiting variable composition (211–214 atoms). The centers of the clusters of the two partial structures define two interpenetrating diamond-like nets, whereas a triply periodic minimal surface (*D* surface) separates the compositionally variable from the invariant part of the structure.

A comprehensive analysis of compositionally distinctive crystals reveals a systematic correlation between the site occupancy factors of partially occupied, mixed-occupied and positional disordered sites. The unravelled correlation between the three types of disorder discloses a before unseen mechanism for the evolution of a homogeneity range in a structurally complex alloy: Instead of the typically observed substitution of atoms we find clear evidence for a mutual substitution of distinctive 26–29 atom clusters. Hence, the homogeneity range arises from an incoherent intergrowth of distinctive partial structures in variable proportions on length scales corresponding to small integers of the approximately 2 nm large cubic lattice parameter. A crystal-chemically meaningful formula is derived which adequately accounts for the compositional flexibility of the phase in structural terms, and for the correlation between three distinctive types of disorder which are reflected in partially occupied, mixed-occupied and split sites. We provide arguments that the linear interdependence of the quantities measuring the various forms of disorder reflect the structure controlling electronic factors in terms of a Hume-Rothery stabilization although the number of electrons per atom deviates significantly from the *vec* value of a typical γ-type phase.

Experimental Section

Synthesis and morphological features: Preparative investigations aiming at the uncovering of Zn-rich phases in the Ir–Zn system were performed on a half gram scale using elemental iridium (99.9%, Merck) and zinc (99.9999%, Chempur). The metals were sealed in previously out-gassed, fused silica ampules under a reduced argon pressure of about 0.5 Pa. The molar fraction x_{Ir} of the mixtures was varied systematically between 0.05 and 0.12. The ampoules were continuously heated up to 1373 K, kept at this temperature for 0.5 h, and subsequently cooled down to 1073 K at a rate of 5 K h^{-1}. After a further annealing for 6 h the silica ampoules were brought to ambient temperature by quenching in cold water. Zinc loss due to vaporization was essentially circumvented by keeping the volume of the reaction vessels small and the condensed sample at the less hot side of the tube. Little amounts of gaseous zinc sometimes re-condensed into few tiny globules close by the brittle, silvery, lustrous metallic regulus accumulating most of the product. In some cases few crystals of vertex-truncated tetrahedral shape and isometric or plate-like habit, sporadically exhibiting oblate edges, were found ranging up to (0.6 mm)^3 in size (Figure 6).

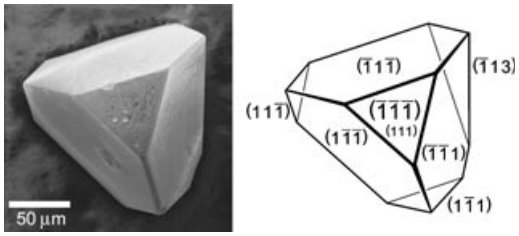

Figure 6. Scanning electron micrograph of a vertex-truncated-tetrahedral shaped single crystal of $Ir_{7+7\delta}Zn_{97-11\delta}$ with isometric habit (crystal 2; x_{Ir} = 0.095, δ = 0.38; point group symmetry $\bar{4}3m$; left side) and its face indexation (right side), as determined for a numerical absorption correction.

X-ray diffraction and EDS measurements revealed that these crystals had the same composition as those quarried out from the buttons. Ir-rich samples (x_{Ir} = 0.12) contained also crystals of truncated octahedral shape. They proved to be the known, ordinary γ-brass-type phase $Ir_{2-x}Zn_{11+x}$,[23] which apparently coexists with $Ir_{7+7\delta}Zn_{97-11\delta}$. Similar reactions performed slightly above the formation temperature of the target phase (1073 K, 60 h) yielded grey, microcrystalline powders. Both procedures are equally suitable for producing single phase samples.

X-ray powder diffraction, chemical and thermal analyses, magnetic and electrical properties: Diffraction patterns of the samples were recorded with a X'Pert MPD X-ray powder diffractometer (Philips) operating in Bragg–Brentano geometry with $Cu_{K\alpha}$ radiation. The diffractometer was equipped with a graphite monochromator at the detector side. A single crystalline silicon disc was used as sample holder. The diffraction profiles of homogeneous $Ir_{7+7\delta}Zn_{97-11\delta}$ samples were quantitatively analyzed by a Rietveld method (Figure 7).[32–34] Positional parameters of the single crystal X-ray structure determination were used as starting parameters for the refinement against the bulk sample X-ray powder data, which was collected in continuous scan mode over a period of 15 h in a 2θ range between 10 and 90°. The refined lattice parameter a = 1822.56(4) pm is in good agreement with the parameters determined on single crystals using a four circle diffractometer (CAD 4B, Enraf–Nonius, cf. Table 3). The re-

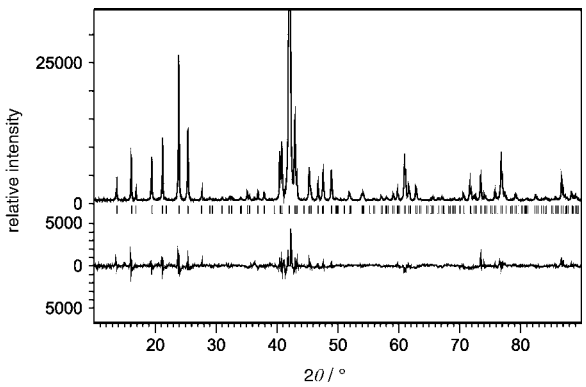

Figure 7. Rietveld analysis of $Ir_{7+7\delta}Zn_{97-11\delta}$ (δ = 0.58). Shown are the observed powder diffraction pattern with the calculated profile function superimposed (25% cutoff for the peak of highest intensity), the Bragg positions and a difference plot (scaled 1.5× relative to the calculated profile function).

Table 3. Crystallographic and technical data for the single crystal structure refinements of $Ir_{7+7\delta}Zn_{97-11\delta}$

	1 (Zn-rich sample)	**2** (intermediate)	**3** (Ir-rich sample)
crystallographic data			
chemical formula	$Ir_{36.22(3)}Zn_{369.79(9)}$	$Ir_{38.35(3)}Zn_{367.3(2)}$	$Ir_{43.96(1)}Zn_{358.94(5)}$
Pearson symbol	*cF*406.0	*cF*405.7	*cF*402.9
x_{Ir}	0.0892	0.0945	0.1091
δ (x_{Ir})	0.31	0.38	0.58
crystal system;			
space group type; Z	cubic; $F\bar{4}3m$ (No. 216); 4		
a/pm[a]	1821.4(2)	1822.4(3)	1822.4(2)
$V/10^6$ pm^3[a]	6042(1)	6052(2)	6052(1)
ρ_{calcd}/g cm^{-3}	8.366	8.496	8.706
μ/mm^{-1}	54.090	55.830	58.536
crystal color	silvery with metallic cluster		
crystal shape	vertex-/edge-truncated tetrahedral, plate-like/isometric habit		
data collection			
crystal size/mm^3	0.09×0.16×0.07	0.12×0.12×0.11	0.15×0.26×0.10
diffractometer	IPDS (Stoe & Cie.)		
radiation	$Mo_{K\alpha}$		
monochromator	graphite		
distance crystal–IP/mm	50	40	40
T/K	293	293	293
$\varphi_{min}-\varphi_{max}$/°	0–256	0–183	0–197
$\Delta\varphi$	1	1	1
$2\theta_{max}$/°	60.76	66.0	66.0
reflns measured	23303	20403	21900
index range	$-25\le h\le 25$ $-25\le k\le 25$ $-25\le l\le 25$	$-27\le h\le 27$ $-27\le k\le 24$ $-27\le l\le 27$	$-26\le h\le 27$ $-27\le k\le 26$ $-27\le l\le 27$
completeness of data set	0.994	0.995	0.995
data reduction			
data reduction/ absorption correction	IPDS-Software,[46] X-RED[35]/ numerical, X-SHAPE[36]		
min/max transmission	0.0275/0.0998	0.0269/0.0884	0.0085/0.0650
unique reflns	951	1185	1179
R_{int}	0.0739	0.0761	0.0926
structure solution, refinement			
structure solution	Direct methods, SHELXS-97[37]		
structure refinement	full-matrix least-squares on F^2 (SHELXL-97[37])		
no. reflns used	951	1185	1179
no. variables	83	91	76
observed reflns ($F_o>4\sigma(F_o)$)	940	1116	1135
$R(F)$ ($F_o>4\sigma(F_o)$)	0.0469	0.0520	0.0350
$R(F)$ (all data)	0.0471	0.0554	0.0363
weighting factor k[b]	0.0609	0.0623	0.0385
$wR(F^2)$ (all data)	0.1406	0.1358	0.0907
GOF (F^2)	2.082	1.690	1.692
extinction coefficient	0.000040(13)	0.000062(11)	0.000070(9)
$\Delta\rho_{min}/\Delta\rho_{max}/10^{-6}$ e pm^{-3}	−3.315/3.816	−2.942/3.768	−2.209/1.864

[a] Parameters determined by use of a four circle diffractometer (cf. Experimental Section). [b] Weighting scheme: $1/\omega = \sigma^2(F_o^2)+(k\cdot P)^2$ with $P = {}^1/_3(\max(F_o^2,0)+2F_c^2)$.

siduals for the final refinement cycle affirm the correctness of the structural model (R_e: 0.0248; R_p: 0.0800; wR_p: 0.1107; R_B: 0.0329; GOF: 4.463; d statistic: 0.580).

The morphology and chemical composition of selected samples were examined in a scanning electron microscope (CS 4DV, CamScan) providing an energy dispersive X-ray spectrometer (EDS, Si(Li)-detector, Noran Instruments). EDS spectra were recorded from those samples which had been studied by means of single crystal X-ray diffraction methods. The emitted X-ray intensities were recorded from 5–10 spots in each case at an accelerating voltage of 20 kV. No impurities of elements heavier than carbon were found to be present in the samples. The analyses confirm the results of the single crystal structure refinements: $x_{Ir}=0.10(2)$ (crystal 1), 0.11(2) (crystal 2), 0.11(1) (crystal 3).

The thermo-chemical properties of two samples ($x_{Ir}=0.085$ and 0.110) were studied in the temperature range 873–1373 K employing a differential scanning calorimeter (DSC, setsys 16/18, Setaram). To suppress decomposition by incongruent vaporization of zinc the cold-pressed samples (30–50 mg, 3.5 mm across) were sealed in previously out-gassed, evacuated silica crucibles which were repeatedly heated and cooled at rates of 10 K h^{-1} with intermediate isothermal treatments at 873 K in order to prove the reversibility of the sluggish cubic/monoclinic transition occurring at about 1045 K upon cooling. The reported transition temperatures result from averaging the temperatures of peak maxima of a thermal event for several heating cycle repetitions. It is noteworthy to mention that the transition temperatures for the two samples did not differ significantly.

Molar magnetic susceptibilities χ_{mol} of three single phase samples $Ir_{7+7\delta}Zn_{97-11\delta}$ (30–60 mg) of nominal compositions $x_{Ir}=0.080$, 0.100, 0.109 were recorded with a SQUID magnetometer (MPMS, Quantum Design) in the temperature range 1.8–330 K at a magnetic flux density of 3 T. The diamagnetic contributions of the sample holder were subtracted from the data. The temperature-independent diamagnetic contributions were determined from the slope of a $\chi_{mol}T$ versus T plot by applying a linear least-square regression to the data.

Electrical resistances of a cold-pressed bar ($8\times2\times0.04\,mm^3$) of single phase $Ir_{7+7\delta}Zn_{97-11\delta}$ ($x_{Ir}=0.100$) were measured with a linear four-probe DC technique. The sample was placed on an electrically insulating mica disc mounted on a copper holder and connected via silver varnish by silver wires (∅: 50 μm, 99.9985 %, Alfa). Contact distances and the cross sectional area of the bar were determined using a light microscope. The voltage was measured at a constant current of 10 mA for temperatures between 12 and 293 K in steps of 1 K. Resistivities ρ were calculated with respect to the sample dimensions ($6\times0.08\,mm^3$).

Single crystal X-ray diffraction and structure determination: Five crystals from samples with different nominal composition ranging from $0.08\leq x_{Ir}\leq0.12$ were studied by X-ray diffraction means. Since the results of two refinements concur with the other ones we confine ourselves to report the data of the three compositionally most distinct phases. The crystal richest in zinc (crystal 1) stemmed from a sample with a nominal composition of $x_{Ir}=0.08$. Ir-rich crystals (e.g. crystal 3) were selected from samples containing γ-Ir_2Zn_{11} as a second component. Crystal 2, having a medium Zn-content, was taken from a sample of nominal composition $x_{Ir}=0.10$. The diffraction intensities were recorded with an image plate diffractometer (IPDS, Stoe & Cie.) operating with $Mo_{K\alpha}$ radiation. The intensities could be indexed conclusively on the basis of a 1.8 nm large *F*-centered cubic unit cell. More reliable lattice parameters for each crystal were determined from the Bragg positions of selected reflections, measured on a four-circle diffractometer (CAD 4B, Enraf–Nonius) at ambient temperatures. The data sets were corrected for Lorentz and polarization effects. A numerical absorption correction based on the precisely measured size of the crystal and its face indexation was applied to the data (cf. Figure 6).[35] In cases where this method was not reliably applicable the internal R value was minimized by empirically varying the size and shape of an originally idealized truncated tetrahedron.[36] The structure was solved in the acentric space group $F\bar{4}3m$ (No. 216) by applying direct methods and subsequently refined on F^2 with a full-matrix least-square algorithm.[37] The possible positions of missing Zn atoms were taken from difference Fourier synthesis maps. At this stage the structure refinements converged at $R(F)$ values somewhat smaller than 0.15. Further improvement of the calculations was achieved by partially replacing iridium for zinc on those Zn sites which showed physically meaningless small or negative displacement parameters, assuming these sites to be fully occupied overall. On the other hand those metal sites with conspicuously enlarged displacement parameters were checked for partial occupancy and positional disorder. Atomic sites for which the refined occupational factors deviated less than twice the standard deviation from unity were considered to be fully occupied. Local structural disorder was adequately accounted for by introducing split positions where peak splitting in electron density maps projected perpendicular to [111] and [10$\bar{1}$] suggested such a treatment and proved to be beneficial for minimizing $R(F^2)$. All disordered sites were refined with non-coupled occupation parameters, except the ones showing mixed occupancy (M22, M23; for example, SOF(Ir22) = 1 − SOF(Zn22)). Each structure was checked for possible twinning by inversion and its absolute configuration. The final refinement including an extinction correction, anisotropic displacement parameters for all atoms, and a proper weighting scheme yields $R(F)$ values between 0.035 and 0.055. Crystallographic data and essential details of the structure refinement are summarized in Table 3. Table 2 lists the positional and occupational parameters together with the equivalent displacement parameters U_{eq}. The anisotropic displacement parameters are visualized by ellipsoids as shown in Figure 3. Further details of the crystal structure investigations can be obtained from the Fachinformationszentrum Karlsruhe, D-76344 Eggenstein-Leopoldshafen, Germany, (fax: (+49) 7247-808-666; e-mail: crysdata@fiz.karlsruhe.de) on quoting the depository numbers CSD-413528 (crystal 1: $Ir_{36.22(3)}Zn_{369.79(9)}$), CSD-413529 (crystal 2: $Ir_{38.35(3)}Zn_{367.3(2)}$) and CSD-413530 (crystal 3: $Ir_{43.96(1)}Zn_{358.94(5)}$).

Acknowledgements

We thank Clemens Pietzonka for recording the magnetic susceptibility data. This research was financially supported by the Deutsche Forschungsgemeinschaft (DFG-Ha 1726/8-1), the National Science Foundation NSF (NSF-DMR-0073587) and the Fonds der Chemischen Industrie.

[1] W. Hume-Rothery, *J. Inst. Met.* **1926**, *35*, 295–361.
[2] W. Hume-Rothery, G. V. Raynor, *The Structure of Metals and Alloys*, Institute of Metals, London, **1954**.
[3] H. Jones, *Proc. Phys. Soc. London* **1937**, *49*, 250–257.
[4] N. F. Mott, H. Jones, *The Theory of the Properties of Metals and Alloys*, Dover, New York, **1958**.
[5] T. B. Massalski, U. Mizutani, *Prog. Mater. Sci.* **1978**, *22*, 151–262.
[6] L. M. Hoistad, S. Lee, *J. Am. Chem. Soc.* **1991**, *113*, 8216–8220.
[7] A. J. Bradley, P. Jones, *J. Inst. Met.* **1933**, *51*, 131–162.
[8] A. J. Bradley, J. Thewlis, *Proc. R. Soc. London Ser. A* **1926**, *112*, 678–692.
[9] S. Mahne, B. Harbrecht, *J. Alloys Compd.* **1994**, *203*, 271–279.
[10] S. Lidin, M. Jacob, A.-K. Larsson, *Acta Crystallogr. Sect. C* **1994**, *50*, 340–342.
[11] F. Bonhomme, K. Yvon, *J. Alloys Compd.* **1995**, *227*, L1–L3.
[12] T. Nash, W. Jeitschko, *J. Solid State Chem.* **1999**, *143*, 95–103.
[13] B. Harbrecht, S. Thimmaiah, M. Armbrüster, C. Pietzonka, S. Lee, *Z. Anorg. Allg. Chem.* **2002**, *628*, 2744–2749.
[14] S. Thimmaiah, K. W. Richter, S. Lee, B. Harbrecht, *Solid State Sci.* **2003**, *5*, 1309–1317.
[15] S. Mahne, F. Krumeich, B. Harbrecht, *J. Alloys Compd.* **1995**, *218*, 177–182.
[16] B. Harbrecht, N. Rheindorf, V. Wagner, *J. Alloys Compd.* **1996**, *234*, 6–11.
[17] M. H. Booth, J. K. Brandon, R. Y. Brizard, C. Chieh, W. B. Pearson, *Acta Crystallogr. Sect. B* **1977**, *33*, 30–36.
[18] M. Conrad, S. Thimmaiah, W. Hornfeck, S. Lee, B. Harbrecht, unpublished results.
[19] A. J. Bradley, J. Thewlis, *Proc. R. Soc. London Ser. A* **1927**, *115*, 456–471.
[20] G. D. Preston, *Phil. Mag.* **1928**, *5*, 1198–1206.
[21] J. A. Oberteuffer, J. A. Ibers, *Acta Crystallogr. Sect. B* **1970**, *26*, 1499–1504.
[22] G. A. Yurko, J. W. Barton, J. G. Parr, *Acta Crystallogr.* **1959**, *12*, 909–911.
[23] L. Arnberg, S. Westman, *Acta Chem. Scand.* **1972**, *26*, 513–517.
[24] E. Hellner, *Struct. Bonding (Berlin)* **1979**, *37*, 61–140.
[25] E. Hellner, E. Koch, *Acta Crystallogr. Sect. A* **1981**, *37*, 1–6.
[26] B. Chabot, K. Cenzual, E. Parthe, *Acta Crystallogr. Sect. A* **1981**, *37*, 6–11.
[27] P. Niggli, *Z. Kristallogr. Krist.* **1922**, *57*, 253–299.
[28] H. A. Schwarz, *Gesammelte mathematische Abhandlungen I*, Springer, Berlin, **1890**.
[29] A. H. Schoen, NASA Technical Note TN D-5541 (1-98), Washington DC, **1970**.
[30] A. L. Mackay, *Chem. Phys. Lett.* **1994**, *221*, 317–321.
[31] P. J. F. Gandy, D. Cvijović, A. L. Mackay, J. Klinowski, *Chem. Phys. Lett.* **1999**, *314*, 543–551.
[32] Philips Analytical, X'Pert Plus (1.0), Almelo, **1999**.
[33] H. M. Rietveld, *Acta Crystallogr.* **1967**, *22*, 151–152.
[34] H. M. Rietveld, *J. Appl. Crystallogr.* **1969**, *2*, 65–71.
[35] X-RED (1.02)-Data Reduction Program. Stoe & Cie., Darmstadt (Germany), **2001**.
[36] X-SHAPE (2.01)-Crystal Optimization for Numerical Absorption Correction. Stoe & Cie., Darmstadt (Germany), **2001**.
[37] G. M. Sheldrick, SHELX-97-A Program Package for the Solution and Refinement of Crystal Structures, Universität Göttingen (Germany), **1997**.
[38] K. A. Brakke, The Surface Evolver (2.20/2003)-Interactive Program for the Study of Surfaces, *Exp. Math. 1(2)*, **1992**, 141–165.
[39] S. Samson, *Acta Crystallogr. Sect. B* **1972**, *28*, 936–945.
[40] L. Westin, L.-E. Edshammar, *Acta Chem. Scand.* **1972**, *26*, 3619–3626.

[41] A. S. Koster, J. C. Schoone, *Acta Crystallogr. Sect. B* **1981**, *37*, 1905–1907.
[42] S. Samson, D. A. Hansen, *Acta Crystallogr. Sect. B* **1972**, *28*, 930–935.
[43] M. L. Fornasini, B. Chabot, E. Parthe, *Acta Crystallogr. Sect. B* **1978**, *34*, 2093–2099.
[44] L. Arnberg, A. Jonsson, S. Westman, *Acta Chem. Scand.* **1976**, *30*, 187–192.
[45] R. Nesper, H.-G. von Schnering, *J. Solid State Chem.* **1987**, *70*, 48–57.
[46] Program Package for X-ray Diffraction, Version 2.75, Stoe & Cie., Darmstadt (Germany), **1996**.

Received: January 19, 2004
Published online: August 3, 2004

